Energy 181 (2019) 239–249

Contents lists available at ScienceDirect

Energy

journal homepage: www.elsevier.com/locate/energy

A numerical study on optimizing the designs of applying PCMs to a disaster-relief prefabricated temporary-house (PTH) to improve its summer daytime indoor thermal environment

Caixia Wang [a, b], Shiming Deng [b, *], Jianlei Niu [b], Enshen Long [a]

[a] Institute for Disaster Management and Reconstruction, Sichuan University, Chengdu, China
[b] Department of Building Services Engineering, The Hong Kong Polytechnic University, Hong Kong SAR, China

ARTICLE INFO

Article history:
Received 4 February 2019
Received in revised form
6 May 2019
Accepted 22 May 2019
Available online 24 May 2019

Keywords:
Disaster-relief
Prefabricated temporary houses
Phase change materials
Thermal environment
Numerical
Optimizing

ABSTRACT

PTHs are massively deployed for disaster-relief after various natural disasters. Following a previous experimental study on applying PCMs to an experimental PTH, where only a very limited number of designs were experimentally examined, in this paper, different designs of applying PCMs to a disaster-relief PTH were numerically examined and the best one identified for guiding future practical applications. A numerical model for a full-scale PTH was established using EnergyPlus and experimentally validated. Using the validated model, a two-part numerical study was carried out. In the first part, a total of 16 different designs were defined and D10 identified as the most effective one, resulting in the highest number of acceptable hours at 90. In the second part, increasing PCM's thickness to beyond 20 mm would lead to negligible effects on further improving indoor thermal environment. Hence, 20 mm thickness was recommended as a reference value for future practical applications. Furthermore, the developed EnergyPlus based model for the experimental PTH may be adapted for other types of PTHs used in different climates. Hence, the outcomes of the numerical study may also guide the future applications of PCM to disaster-relief PTHs of various configurations, and located in different climates.

1. Introduction

After natural disasters that destroy human habitats [1], such as earthquakes, tsunamis, floods, typhoons and bushfires, prefabricated temporary houses (PTHs) are massively used in disaster relief reconstructions [2–5]. For example, after the 2008 mega-scale Wenchuan Earthquake in China, more than 21 million victims were resettled in PTHs during the post-disaster transitional period of up to 36 months, as shown in Fig. 1. Very often, such fast-installed PTHs were the only choice for disaster victims during a post-disaster transitional period, which may nonetheless last for up to several years [6–9]. Furthermore, given the temporary nature, no indoor thermal environmental control systems are usually installed inside PTHs and therefore, their indoor thermal environments are cold in winter and hot in summer [10]. Such a long-term poor indoor thermal environment may result in physical and mental illness of PTHs' occupants, especially those disaster victims [11]. Therefore, improving the indoor thermal comfort for the occupants in PTHs using simple and low-cost measures, such as passive designs [12,13], is urgently needed.

On the other hand, various studies have shown that the use of phase change materials (PCMs) could help improve the indoor thermal comfort in different buildings due to the effect of latent heat storage and release [14]. For instance, Sage-Lauck et al. [15] evaluated the impact of using PCMs on indoor thermal environment in a super-insulated residential building using experimental and numerical approaches. Figueiredo et al. [16] used different constructions incorporating with PCMs in academic buildings and assessed the indoor thermal comfort as real case studies. Alam et al. [17] completed a comparative analysis on the effectiveness of different methods to apply PCMs to residential buildings for increasing indoor thermal comfort.

Although PCMs have been widely applied to various permanent buildings [18–30] as passive measures for improving indoor thermal environments [31], their full-scale applications to temporary disaster-relief PTHs are seldom reported. This may be due to the temporary nature of PTHs since they are not expected for long term use. However, the actual use of PTHs may no longer be temporary

* Corresponding author.
E-mail address: besmd@polyu.edu.hk (S. Deng).

https://doi.org/10.1016/j.energy.2019.05.165
0360-5442/

Nomenclature

T_i	The air temperature inside a PTH, °C
T_o	Outdoor air temperature, °C
T_E	Internal surface temperature of PTH's east wall, °C
T_W	Internal surface temperature of PTH's west wall, °C
T_S	Internal surface temperature of PTH's south wall, °C
T_N	Internal surface temperature of PTH's north wall, °C
T_R	Internal surface temperature of PTH's roof, °C
T_F	Internal surface temperature of PTH's floor, °C
T_{Mt}	Measured temperature at each hour, °C
T_{St}	Simulated temperature at each hour, °C
$\bar{y}$	Average measured temperature during the entire measurement period, °C
AVE_{day}	Average air temperature inside the PTH during 8:00–20:00, °C

Abbreviations

PTHs	Prefabricated temporary houses
PCM	Phase change material
PESS	Phase change material energy storage system
RMSD	Root Mean Square Deviation
$CV_{(RMSD)}$	Coefficient of Variation of root mean square deviation

Fig. 1. Prefabricated temporary houses extensively used in disaster relief after the 2008 Wenchuan Earthquake in China.

following some mega-scale natural disasters, such as the 2008 Wenchuan Earthquake. It therefore becomes highly necessary to investigate the applications of PCMs to PTHs for improving indoor thermal environment, for the well-beings of PTHs' occupants, most of them being disaster victims.

An experimental study on applying PCMs to disaster-relief PTHs was previously reported by the authors [6]. The study results demonstrated that the use of PCMs could help improve the thermal comfort in disaster-relief PTHs effectively at daytime in summer. Two different designs of applying PCMs to disaster relief PTHs for improving their internal thermal environments at daytime in summer were experimentally compared and a movable PCM based energy storage system (PESS) was preferred due to its flexibility of utilizing cooling energy from both cold outdoor air and sky radiation at nighttime for discharging the stored heat absorbed from indoor air at daytime, when the PESS was moved to outdoors. However, as limited by the nature of an experimental study, only very limited number of designs for the PESS used in PTHs with a fixed amount of PCM were experimentally examined. Hence, aiming at improving the thermal environment inside PTHs at daytime in summer using PCMs, it becomes highly necessary to optimize the designs of applying PCMs to disaster-relief PTHs. To this end, as a follow-up to the previously reported experimental study [6], a numerical study on optimizing the designs of applying PCMs to a full-scale PTH has been carried out and the study results are reported in this paper. The methodology used in this paper was as follows. Firstly, a numerical model for the full-scale experimental PTH in the previous experimental study using the well-known building energy simulation platform, EnergyPlus, was established, and experimentally validated using the data collected from the experimental PTH, and weather data in Chengdu. Secondly, using the validated model, two parts of the numerical study, i.e., evaluating different designs of applying PCMs to the PTH and examining the effects of different amounts of PCM to be used, were carried out. Thirdly, the numerical study results were analyzed for identifying the best design of applying PCM to PTHs.

2. Model development and validation

2.1. Model establishment

A simulation model for a full-scale PTH was established using the famous building thermal load and energy analysis simulation platform, EnergyPlus [32–38], which has been extensively used in indoor thermal environmental analysis and building energy efficiency evaluation. EnergyPlus could be used to evaluate the thermal loads and energy consumption of a building based on its physical configurations and details of HVAC installations, and can be applied to both conditioned and unconditioned buildings. In the current numerical study, the algorithm of CondFD in EnergyPlus was selected to simulate the heat transfer of PCM in the PTH. The temperature of PCM at each time interval could be calculated iteratively according to a first-order full implicit differential heat transfer method.

The model developed in this study was based on a full-scale experimental PTH used in the previous experimental study [6], as shown in Fig. 2.

2.2. The experimental PTH

In the simulation study using EnergyPlus, a PTH was modelled based on characteristics of the experimental PTH, including size, orientation, configuration, materials and surroundings, etc. The size of the full-scale experimental PTH was 5.6 m × 3.8 m × 2.7 m with two 1.7 m × 0.9 m windows and one 2.0 m × 0.8 m door. It was made of light-weight prefabricated insulation panels and wood. It represented those typical conventional PTHs in the current Chinese market, in terms of both dimensions and envelope materials. The full-scale experimental PTH was placed on the roof top of a four-story building in the campus of Sichuan University. A movable PESS was placed near the west wall inside the full-scale experimental PTH, as shown in Fig. 3. Totally, there were 1240 tubes which were horizontally tiled onto plastic net-shape containers in the PESS, and each container was suspended on a steel shelf during the experimental study period in the PTH. In addition, since the PESS was movable, experiments can be carried out with and

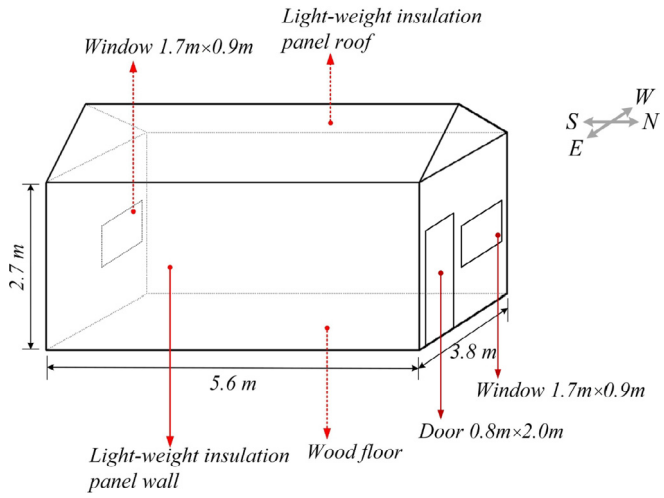

Fig. 2. A 3-D illustration of the full-scale experimental PTH.

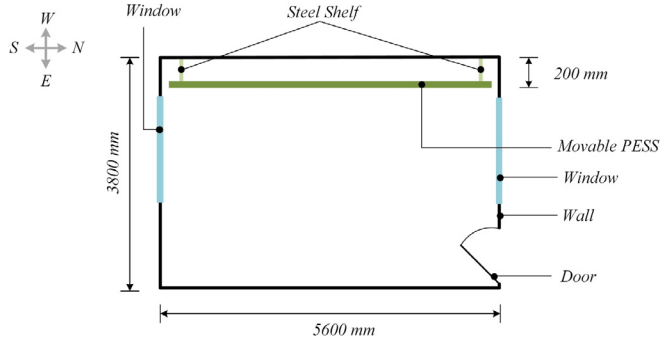

Fig. 3. Top view of the PESS placed inside the full-scale experimental PTH.

without the PESS placed inside the full-scale PTH for comparison purposes. The details of envelope materials, the physical and thermal properties of these envelope materials and the physical and thermo-physical parameters of PCMs are given in Tables 1–3, respectively.

2.3. Model validation

The indoor air temperature and internal surface temperatures of four walls, roof and floor of the experimental PTH were measured for the purpose of model validation. As shown in Fig. 4, eight number of thermocouples were placed inside the experimental PTH. These eight thermocouples were located at the center of the full-scale PTH, with a distance of 300 mm between any two of them. The indoor air temperature of the experimental PTH (T_i) was obtained by averaging the readings from the eight thermocouples. Furthermore, T-type thermocouples for measuring the internal surface temperatures of envelopes were also located at the center of the internal surface at each envelope component. The measuring accuracy for the thermocouples was at ± 0.5 °C.

Table 1
Materials of building envelope used in the full-scale experimental PTH.

Building envelope	Materials
Roof and external walls	Steel Expanded polystyrene board
Floor	Wood

In addition, the following weather parameters were recorded by a meteorological and weather station nearby: dry bulb air temperature, air dew point temperature, air relative humidity, atmospheric pressure, extra-terrestrial horizontal radiation, extra-terrestrial direct normal radiation, horizontal infrared radiation intensity from sky, global horizontal radiation, direct normal radiation, diffuse horizontal radiation, global horizontal illuminance, direct normal illuminance, diffuse horizontal illuminance, zenith luminance, wind direction, wind speed, total sky cover and opaque sky cover.

All the measuring instruments were calibrated before they were used in the experiments, and were connected to data loggers where all the measured parameters were recorded at an interval of 5 min. The measurements were taken in the summer from June to September, 2016, typical summer period in Chengdu city, to collect data for model validation.

The EnergyPlus based simulation model established was validated by the collected experimental data. As shown in Fig. 5 and Fig. 6, the simulated parameters of indoor air temperature, internal surface temperature of the west wall, roof and floor of the experimental PTH, with and without the PESS placed inside the PTH, also during the period from June to September, 2016, were compared with the measured ones.

Fig. 5 shows the comparisons between the measured and simulated indoor air temperatures, internal surface temperatures of west wall, roof and floor of the experimental PTH without the PESS placed inside during three selected days of the entire measurement period. As seen, both the measured and simulated indoor air temperatures, internal surface temperatures were increased at daytime, and decreased at nighttime. Good agreements between the measured and simulated temperatures were achieved.

Fig. 6 shows the comparisons between the measured and simulated indoor air temperatures, internal surface temperatures for west wall, roof and floor of the experimental PTH with the PESS placed inside during another three days. The PESS were placed near the west wall inside the experimental PTH throughout the three days. As seen, both the measured and simulated indoor air temperatures, internal surface temperatures for west wall, roof and floor were also increased at daytime, and decreased at nighttime. Again, good agreements between the measured and simulated temperatures were also achieved.

In addition, all the simulated and measured maximum and minimum indoor air and internal surface temperatures of the PTH's envelopes and their variation ranges are listed in Table 4 without, and Table 5 with the PESS placed inside the PTH, respectively.

As seen from Tables 4 and 5, both the simulated values and the measured values were close to each other, suggesting the acceptable accuracy of simulated results.

In order to ensure the validation accuracy, two metrics: Root Mean Square Deviation (RMSD) and Coefficient of Variation ($CV_{(RMSD)}$), were employed. While RMSD measured the average spread of errors which provided a measure for model's dispersion [39], $CV_{(RMSD)}$ was the coefficient of variation in RMSD, as expressed by Eqs. (1) and (2), respectively, as follows:

$$RMSD = \sqrt{\frac{1}{N}\sum_{t=1}^{N}(T_{Mt} - T_{St})^2} \quad (1)$$

$$CV_{(RMSD)} = \frac{RMSD}{\bar{y}} \quad (2)$$

where T_{Mt} and T_{St} are the respective measured and simulated temperatures at each hour, t, °C, N the total number of hours, and $\bar{y}$,

Table 2
Physical and thermal properties of the envelope materials used in the full-scale experimental PTH.

Materials	Thickness (mm)	Thermal conductivity (W/m·K)	Density (kg/m^3)	Specific heat (J/kg·K)
Steel	0.5	45.28	8000	460
Expanded polystyrene board	75	0.035	20	1100
Wood	13	0.15	521	1630

Table 3
Thermo-physical properties of the PCM used.

Property	Value
Base material	Inorganic salts
Phase change temperature (°C)	18–26
Operating temperature range (°C)	0–60
Latent heat (kJ/kg)	216
Specific heat capacity (J/(kg·K))	1785
Thermal conductivity (solid) (W/(m·K))	0.5
Thermal conductivity (liquid) (W/(m·K))	0.25
Density at (16–28 °C) (kg/m^3)	1300
Total enthalpy at 16–28 °C (heating) (kWh/m^3)	50
Total enthalpy at 16–28 °C (cooling) (kWh/m^3)	58
Encapsulation material	Aluminum composite membrane
Flammable	Nonflammable
Toxicity	Non-toxic

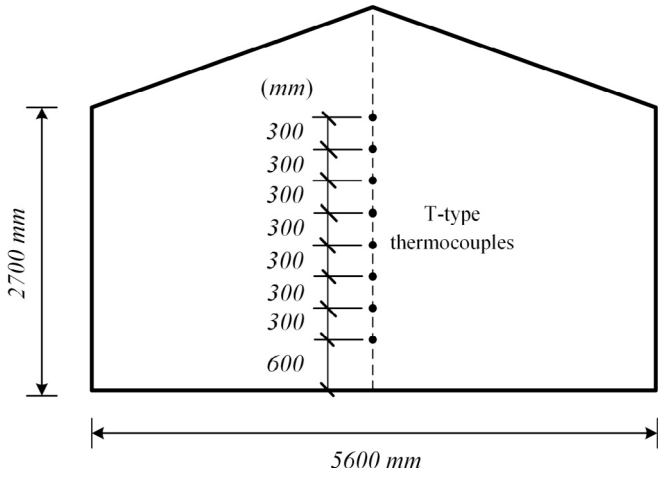

Fig. 4. The locations of T-type thermocouples inside the full-scale experimental PTH.

the average measured temperature during the entire measurement period, °C.

The RMSD and $CV_{(RMSD)}$ for indoor air temperature, and internal surface temperatures for all envelopes of the PTH, with and without the PESS placed inside were calculated and the calculated results are shown in Table 6. As seen, the highest RMSD value of 1.89 °C and $CV_{(RMSD)}$ value of 5.9% were for the air temperature inside the experimental PTH. The $CV_{(RMSD)}$ values were all less than 6%, suggesting that the model developed can be used to predict the thermal environment in terms of indoor air temperature and internal surface temperatures inside the PTH well, with an acceptable accuracy. Therefore, the model can be considered validated and may be used in the numerical study for both optimizing the designs of applying PCMs to a PTH and examining the amount of PCM to be used to improve its indoor daytime thermal environment in summer.

2.4. Model applications

A mathematical model for the experimental PTH was developed using the EnergyPlus platform and experimentally validated. Although the developed model was based on the geometry parameters of the experimental PTH, these parameters may be altered so that the model can be easily adapted for simulating PTHs of different geometries or configurations. On the other hand, although the current numerical study was based on the climate parameters in Chengdu, China, the developed model may also be used in other weather zones when their climate parameters are used.

3. The numerical study

Using the validated model reported in Section 2, a numerical study on optimizing the designs of applying PCMs and examining the amount of PCM to be used, to a PTH located in Chengdu city, Sichuan Province, China, for improving its indoor thermal environment at daytime in summer, has been carried out and the study results are presented in this Section.

3.1. Assumptions used in the numerical study

The period of simulation was from June to September, which is the representative period of summer in Chengdu, China, using the weather data of Chengdu City [41]. Furthermore, the simulation study was carried out under the following assumptions:

- The PTH was occupied by 3 average adults (of 1.73 m tall, 70 kg, DuBois area = 1.8 m^2) [42];
- The activity level of the occupants was at 60 W/m^2 (1.0 met) [43];
- The thermos-physical properties of the PCM used were the same as those shown in Table 3;
- The PCM of 20 mm thickness was sandwiched by two 0.5 mm steel sheets as a PCM panel;
- The hourly internal heat gains from lighting and electric appliance remained constant at 100 W;
- The windows and door of the PTH remained closed throughout the simulation period.

The numerical study included two parts: 1) optimizing the designs of applying PCM to the PTH, and 2) examining the amount of

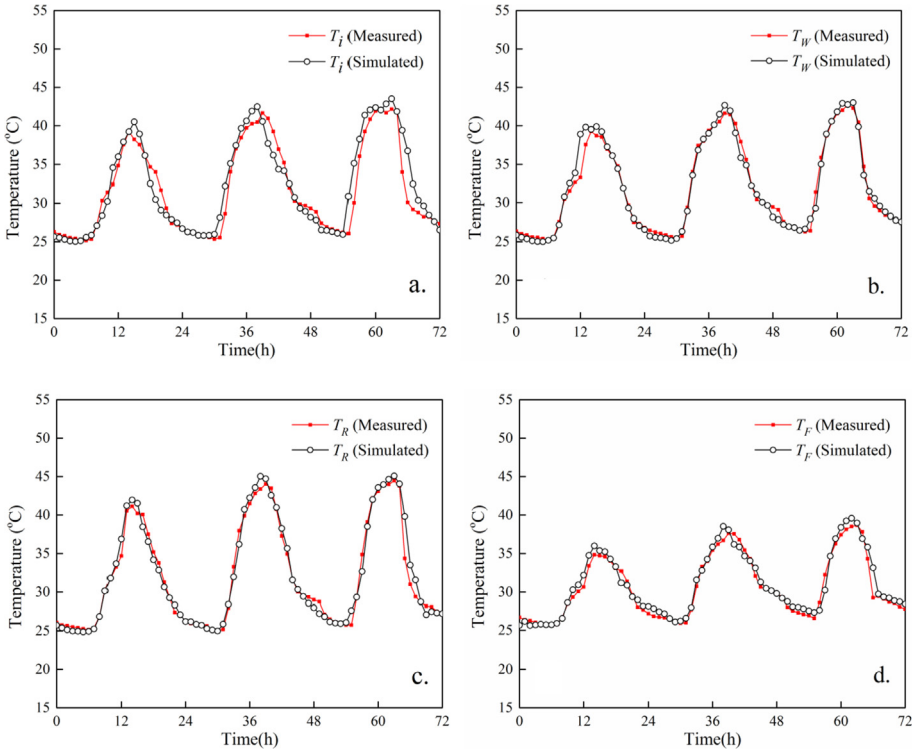

Fig. 5. Comparisons between the measured and simulated a) indoor air temperatures; b) internal surface temperatures of west wall; c) internal surface temperatures of roof; d) internal surface temperatures of floor inside the PTH, without the PESS placed inside.

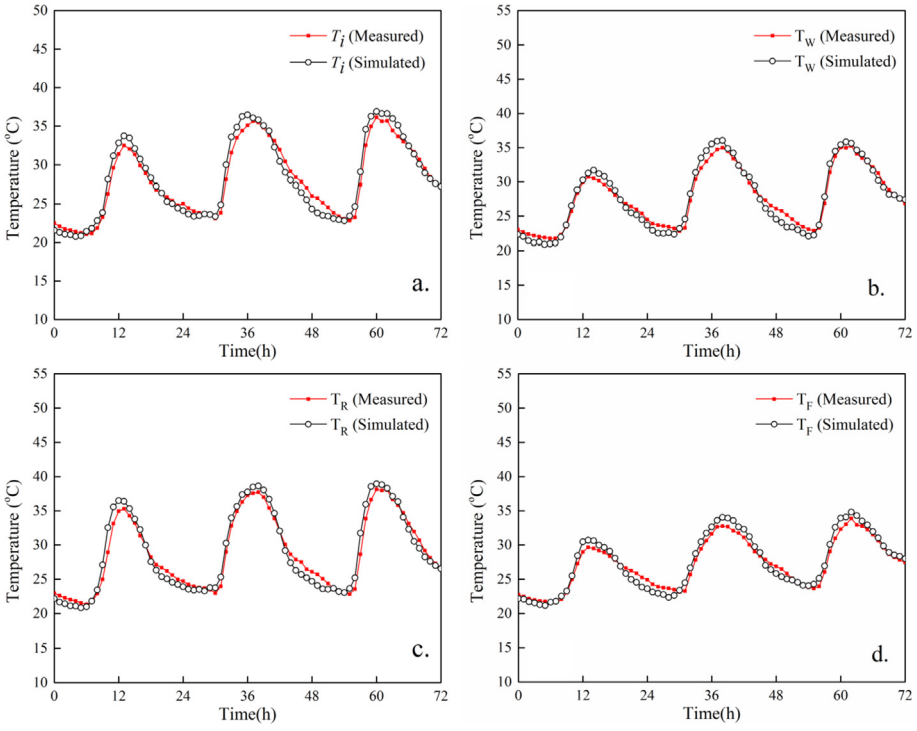

Fig. 6. Comparisons between the measured and simulated a) indoor air temperatures; b) internal surface temperatures of west wall; c) internal surface temperatures of roof; d) internal surface temperatures of floor inside the PTH, with the PESS placed inside.

PCM used. The study results for the two parts are presented in Sections 3.2 and 3.3, respectively.

3.2. Optimizing the designs of applying PCM to the PTH

In the previously reported experimental study [6], only the

Table 4
Simulated and measured maximum and minimum indoor air and internal surface temperatures and their variation ranges without the PESS placed inside the PTH.

Measured	T_i	T_E	T_W	T_S	T_N	T_R	T_F
Maximum	42.17	42.73	42.75	43.52	43.23	44.45	38.65
Minimum	25.16	25.42	25.28	25.64	25.02	25.09	25.61
Variation range	17.01	17.31	17.47	17.88	18.21	19.35	13.04
Simulated	T_i	T_E	T_W	T_S	T_N	T_R	T_F
Maximum	43.51	43.12	43.01	43.16	43.92	45.08	39.57
Minimum	25.02	25.04	25.00	25.19	24.87	24.85	25.62
Variation range	18.49	18.08	18.01	17.97	19.05	20.23	13.95

Table 5
Simulated and measured maximum and minimum indoor air and internal surface temperatures and their variation ranges with the PESS placed inside the PTH.

Measured	T_i	T_E	T_W	T_S	T_N	T_R	T_F
Maximum	36.17	36.12	36.05	36.63	36.28	38.13	33.88
Minimum	21.08	20.83	20.90	21.16	21.02	21.35	21.64
Variation	15.08	15.29	15.15	15.47	15.26	16.78	12.23
Simulated	T_i	T_E	T_W	T_S	T_N	T_R	T_F
Maximum	36.90	36.49	36.23	36.49	36.43	38.93	34.81
Minimum	20.77	20.85	20.75	20.44	20.51	20.83	21.17
Variation	16.31	15.64	15.48	16.05	15.92	18.10	13.64

design for the PCM located near the indoor side of the PTH's west wall was examined. However, whether this design was the best remained to be examined when locating the PCM at different positions inside or outside the PTH. Hence, optimizing the designs of applying PCM at different positions inside and outside the PTH was numerically studied.

Therefore, various designs of locating the PCM in different positions relative to the PTH's envelopes were firstly defined. As shown, PCM was located on the outdoor side and the indoor side of the roof, as Position ①, ② and ③ in Fig. 7a, b and 7c, respectively. Furthermore, PCM was located on the outdoor side and the indoor side of a wall, as Position ④, ⑤ and ⑥ of the walls, as shown in Fig. 8a, b and 8c, respectively. Consequently, a total of sixteen different designs for locating the PCM at different positions, i.e., D1 to D16, were hence defined, as detailed in Table 7.

As examples, the simulated air temperatures inside the PTH in D1, D 11–13, together with outdoor air temperature over a total of four selected days within the period of simulation, are shown in Fig. 9 and Fig. 10, respectively. In Fig. 9, the outdoor air temperature and the simulated indoor air temperature in D1, T_o and $T_{i\ (D1)}$, are shown. As seen, during the four days, the indoor air temperature inside the PTH in D1, $T_{i\ (D1)}$, varied from 18.87 °C to 41.77 °C, and $T_{i\ (D1)}$ was always higher than T_o at daytime. Clearly, there was a similar trend in the variation patterns for both outdoor air temperature and the simulated indoor air temperature. However, due to the solar heat gain and without ventilation at daytime, indoor air temperature in D1 could be much higher than outdoor air temperature. For example, when the highest outdoor air temperature was 31.1 °C on the second day, indoor air temperature was at 41.77 °C due to the solar heat gain, and without ventilation. Hence, air temperature inside the PTH was intolerably high [40] throughout most of the daytime on that day. Furthermore, indoor air temperature at nighttime on the four simulation days was only just slightly lower than outdoor air temperature.

In Fig. 10, the simulated indoor air temperatures in D 11–13, $T_{i\ (D11)}$, $T_{i\ (D12)}$ and $T_{i\ (D13)}$, are shown. In D11, PCM was located outside south wall of the PTH, 200 mm away from its external surface. In D12, PCM was placed outside the PTH close to the outside surface of south wall. In D13, PCM was located close to the indoor side of south wall and was moved to outside of the PTH from 20:00 to 8:00 on the following day, for releasing the absorbed heat at night to low temperature outdoor air at nighttime. As seen, during the four days, the simulated indoor air temperature in D13, $T_{i\ (D13)}$, varied from 18.91 °C to 37.76 °C, the lowest at both daytime and nighttime among the three designs. This suggested that the use of PCM on a movable base, which was placed on the indoor side of the south wall at daytime could help improve the thermal environment inside the PTH more effectively when compared with the use of PCM in both D11 and D12 at daytime. At nighttime, the simulated results demonstrated that $T_{i\ (D13)}$ exhibited similar variation profile with $T_{i\ (D11)}$ because PCM was moved to outside of the PTH at nighttime, and $T_{i\ (D12)}$ was higher than $T_{i\ (D11)}$ and $T_{i\ (D13)}$ at nighttime because heat was released from the PCM on the external surface of the south wall and transferred into indoor via conduction through the wall.

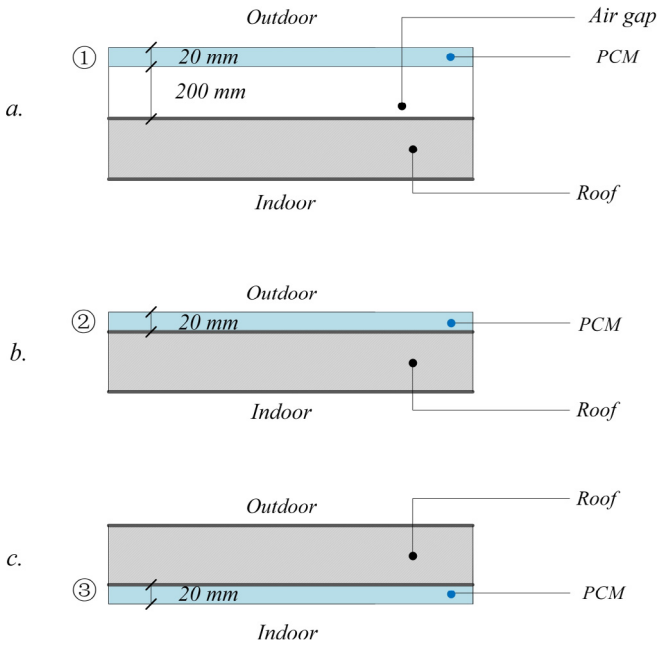

Fig. 7. Different positions of the PCM relative to the roof of the PTH.

Table 6
Summary of RMSD and $CV_{(RMSD)}$, both with and without the PESS placed inside the PTH.

Without the PESS placed inside the PTH							
Parameters	T_i	T_E	T_W	T_S	T_N	T_R	T_F
RMSD	1.89	0.99	1.07	1.12	1.25	1.10	0.90
$CV_{(RMSD)}$	5.9%	3.1%	3.4%	3.6%	4.0%	3.4%	2.9%
With the PESS placed inside the PTH							
Parameters	T_i	T_E	T_W	T_S	T_N	T_R	T_F
RMSD	1.04	0.91	0.91	0.97	1.03	1.17	0.92
$CV_{(RMSD)}$	3.7%	3.3%	3.2%	3.4%	3.5%	4.0%	3.3%

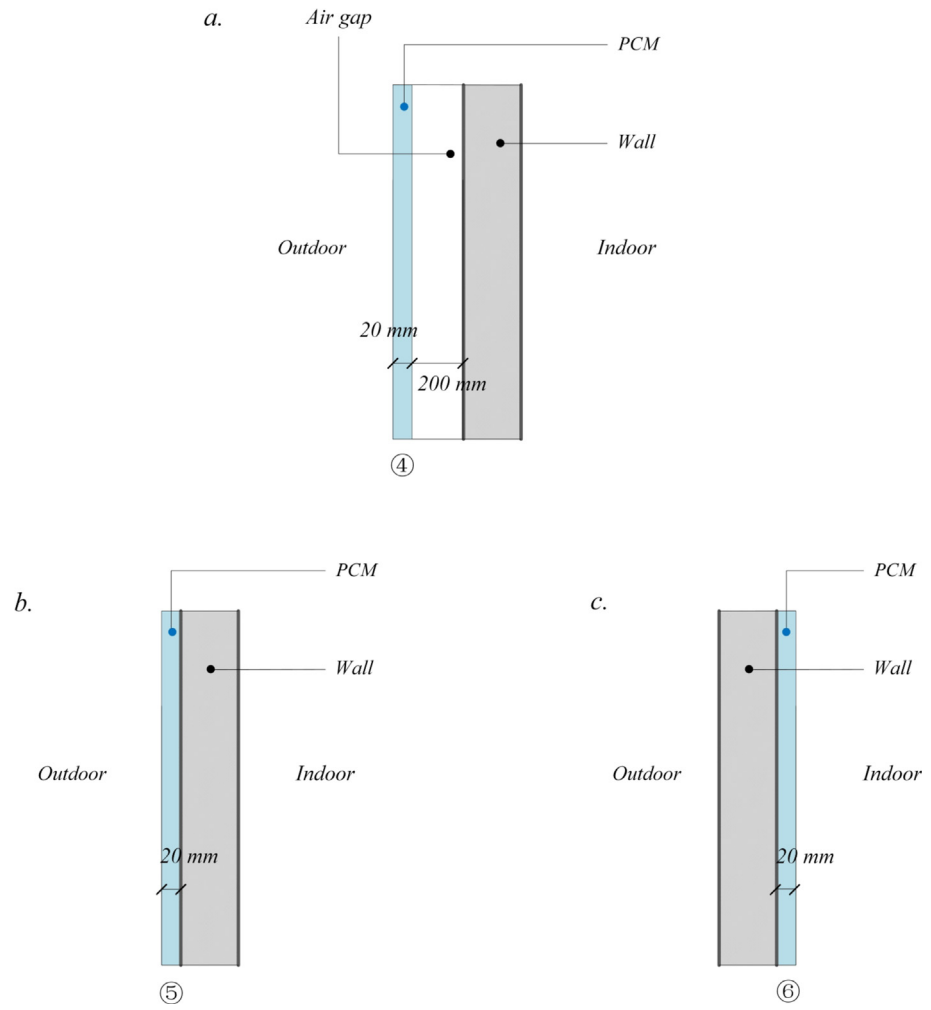

Fig. 8. Different positions of the PCM relative to a wall of the PTH.

Table 7
Details of the sixteen designs.

Design	Details
1	Without PCM- Baseline design
2	PCM always at ① for Roof
3	PCM always at ② for Roof
4	PCM at ③ for Roof at daytime, but moved to outside the PTH at nighttime
5	PCM always at ④ for East Wall
6	PCM always at ⑤ for East Wall
7	PCM at ⑥ for East Wall at daytime, but moved to outside the PTH at nighttime
8	PCM always at ④ for West Wall
9	PCM always at ⑤ for West Wall
10	PCM at ⑥ for West Wall at daytime, but moved to outside the PTH at nighttime
11	PCM always at ④ for South Wall
12	PCM always at ⑤ for South Wall
13	PCM at ⑥ for South Wall at daytime, but moved to outside the PTH at nighttime
14	PCM always at ④ for North Wall
15	PCM always at ⑤ for North Wall
16	PCM at ⑥ for North Wall at daytime, but moved to outside the PTH at nighttime

Similar to the results shown in Fig. 10 for the south wall, locating the PCM on the indoor side of the other walls and moving it to outside the PTH could also help improve the thermal environment in the PTH more than the use of PCM on the outdoor side of the walls at daytime.

The simulated results for D 2–16 suggested that locating the PCM on the indoor side of roof and the four walls, i.e., in D4, D7, D10, D13 and D16, could help improve the thermal environment in the PTH more than locating PCMs on the outdoor side of roof and the four walls at daytime. In addition, in these designs, as the PCM may be moved to outside the PTH at nighttime, the use of PCM at daytime would not, therefore, impair the thermal environment

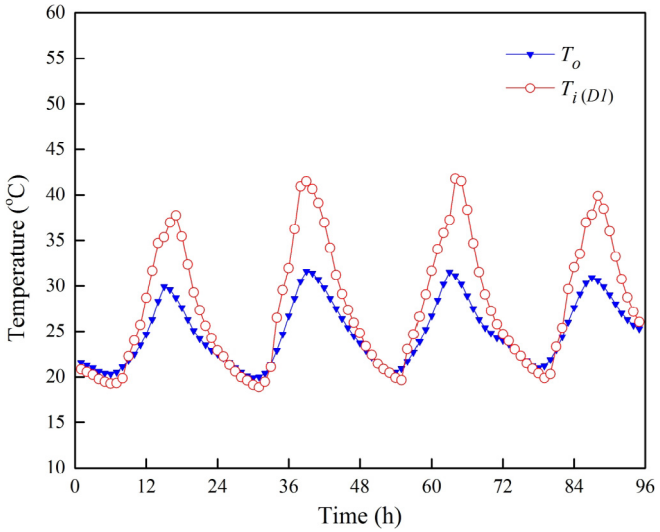

Fig. 9. The outdoor air temperature and simulated indoor air temperature over the four selected days in D1.

inside PTH at nighttime. Hence, the design of a movable PESS like that used in the previous experimental study [6], was preferred. The simulated results clearly demonstrated that a movable PESS may be used to help eliminate the negative effect of placing PCM inside the PTH at nighttime, while it can effectively improve the thermal environment in the PTH at daytime.

The simulated maximum and minimum T_o and T_i in D 1–16 are shown in Table 8. As seen, as compared to those for D1, all the maximum values of T_i in D 2–16 were lower, suggesting the effect of using PCM for improving indoor thermal environment at daytime in summer. However, there was a large variation in the 16 maximum T_i values, from 36.61 °C in D10 to 41.77 °C in D1, i.e., the baseline design. On the other hand, in D 2–16, their minimum values of T_i stayed relative stable with a small variation range from 18.87 °C in D10 to 19.88 °C in D3. Furthermore, the average T_i in D10 was the lowest at 26.9 °C. These further suggested that, again, the use of PCM on the indoor side of roof and four walls was more effective for improving the thermal environment at daytime inside the PTH than on the outdoor side of roof and four walls. Furthermore, the designs with PCM to be moved to outdoor were more

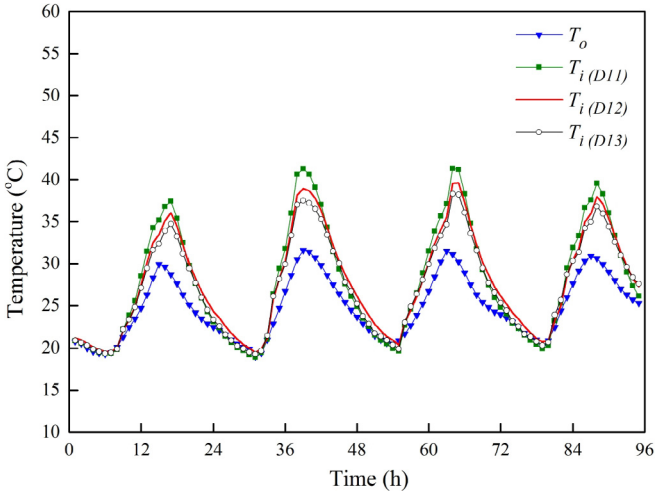

Fig. 10. The simulated indoor air temperatures in D 11-13.

Table 8
Simulated maximum and minimum T_o and T_i for D1-16.

	T_o	$T_{i\,(D1)}$	$T_{i\,(D2)}$	$T_{i\,(D3)}$	$T_{i\,(D4)}$	$T_{i\,(D5)}$
Maximum	31.60	41.77	40.80	37.92	37.84	41.50
Minimum	19.90	18.87	18.96	19.88	19.01	18.91
Average	24.84	27.76	27.69	27.57	27.13	27.76
	$T_{i\,(D6)}$	$T_{i\,(D7)}$	$T_{i\,(D8)}$	$T_{i\,(D9)}$	$T_{i\,(D10)}$	$T_{i\,(D11)}$
Maximum	39.03	37.45	41.64	39.05	36.61	41.33
Minimum	19.74	18.92	18.92	19.73	18.93	18.90
Average	27.70	26.93	27.77	27.69	26.90	27.76
	$T_{i\,(D12)}$	$T_{i\,(D13)}$	$T_{i\,(D14)}$	$T_{i\,(D15)}$	$T_{i\,(D16)}$	
Maximum	39.62	37.76	41.71	39.85	37.73	
Minimum	19.51	18.91	18.90	19.52	18.92	
Average	27.70	27.08	27.76	27.71	27.04	

effective for improving the thermal environment inside the PTH than placing PCM near outdoor side of four walls at both daytime and nighttime. This was because while the use of a design with movable PCM could help not only reduce the air temperature inside the PTH at daytime, but also eliminate the negative effect of placing the PCM inside the PTH at nighttime. Hence a movable PESS design such as that used in the experimental study [6] provided a convenient way to move PCM from indoor to outdoor at nighttime, so as to eliminate the heat release from the PCM to indoor and re-charge the PCM with cooling energy from both the sky radiation and a low temperature outdoor air at nighttime.

The simulated resultant thermally acceptable hours and their normalized percentages out of the total simulation hours inside the PTH for all the designs are shown in Fig. 11. A thermally acceptable hour was defined as an hour during which indoor air temperature inside a PTH was below the occupants' tolerant temperature in temporary shelters after natural disasters at 34 °C [40]. As seen, compared with the baseline design, the values of acceptable hours and the percentage for D10 were 90 h and 93.8%, respectively, during the four days, the highest among all the designs. This was consistent with the simulation results that D10 would lead to the lowest averaged indoor air temperature at 26.9 °C, among all the designs.

3.3. The amount of PCM to be used

It is obvious that the more PCM is used, the greater improvement in indoor thermal environment may be expected. However, the amount of PCM used would have a financial impact on applying

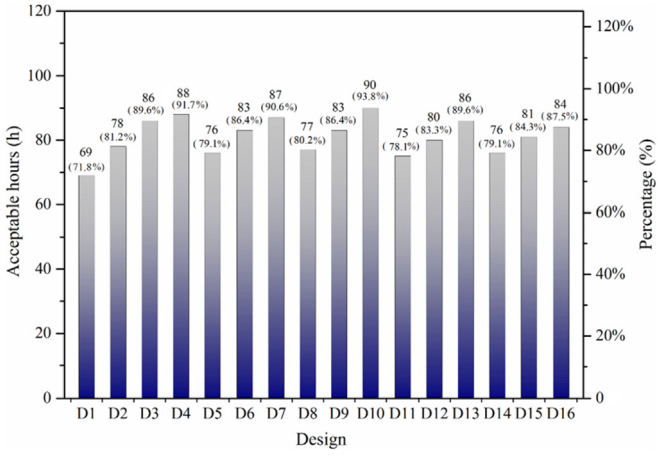

Fig. 11. Simulated thermally acceptable hours and their normalized percentages for D1-D16.

PCM to PTHs. Hence, the numerical study reported in this paper also covered an analysis on the impacts of the amount of PCM used on the thermal environment inside a PTH in summer, which is reported in this section. To simplify the analysis, the amount of PCM used was indirectly represented by its thickness.

From the simulated results shown in Section 3.2, it can be seen that D10 was the most effective design on improving the PTH's indoor thermal environment at daytime in summer among the 16 designs, and hence selected to exam the relationship between the amount of the PCM used and the improvements in the thermal environment inside a PTH. Seven different levels of PCM thickness at 0, 5 mm, 10 mm, 20 mm, 30 mm, 40 mm and 50 mm, were used in the analysis, with 0 mm thickness representing the baseline design.

Table 9 shows the analysis results. As seen, the maximum indoor air temperatures, average indoor air temperatures and daytime average indoor air temperatures (from 8:00 to 20:00) inside the PTH were decreased with the increase in PCM's thickness. On the other hand, the rates of the decreases in these temperatures at different levels of thickness are shown in Fig. 12. As illustrated, the changes in these temperatures at 0–20 mm PCM thickness were greater than those at 20–50 mm PCM thickness. More remarkably, the rates of decrease in these temperatures at 20–50 mm PCM thickness, were fairly small and almost stayed unchanged at 30–50 mm PCM thickness. Therefore, increasing PCM's thickness 1) from 0 mm to 20 mm, would have an obvious impact on regulating PTH's indoor thermal environment, and 2) to beyond 20 mm thickness, would have negligible impacts on further improving PTH's indoor thermal environment. Hence, the PCM thickness of 20 mm may be taken as a reference design value for future practical applications.

With the identified reference design PCM thickness of 20 mm, D10 was further revised to D17 by placing PCM of 20 mm thickness on the indoor sides of roof and all four walls of the PTH at daytime, with the PCM to be moved to outside the PTH at nighttime. As shown in Table 10, the simulated maximum T_i was reduced from 36.61 °C in D10 to 32.30 °C in D17, and the daytime average temperature from 28.93 °C in D10 to 26.82 °C in D17. Hence, these results suggested that it would be more effective to distribute a fixed amount of PCM to all envelope surfaces, rather than simply increasing the amount of PCM for just one particular envelope element.

It should however be noted that this identified 20 mm thickness for PCM was specific for the identified D10 case. For all other cases, further studies should be carried out to find their respective optimal thickness.

3.4. Comparison between the best design identified by simulation and the fixed design used in the experimental study

In this Section, D18 was further defined, which was the fixed design used in the previous experimental study. For D18, the PCM was fixed on the indoor side of the west wall, with a thickness of 20 mm, the same as that for D10. The difference between D10 and D18 was that the PCM layer in D10 could be moved to the outside of a PTH, but that in D18 could not.

Table 9
Simulated maximum and average *Ti* in D10 at different thickness PCM.

PCM's thickness	0	5 mm	10 mm	20 mm	30 mm	40 mm	50 mm
Maximum	41.77	39.80	38.39	36.61	36.21	36.13	36.05
Average	27.76	27.43	27.12	26.90	26.24	26.18	26.14
AVE_{day}	33.63	31.64	30.29	28.93	28.28	27.86	27.53

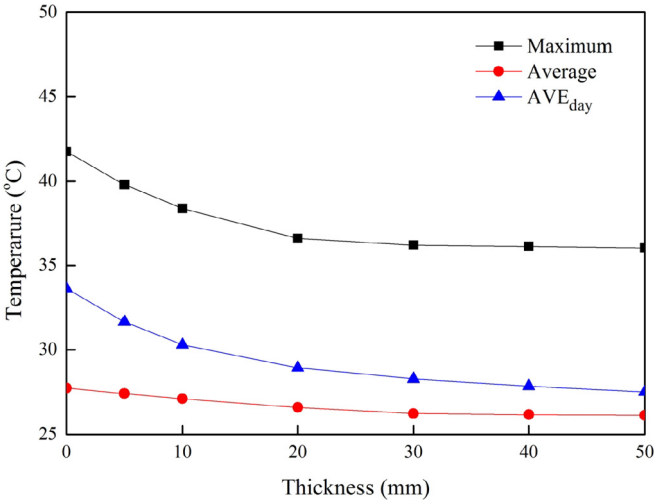

Fig. 12. Simulated rates of decrease in indoor air temperatures at different levels of PCM thickness.

Table 10
Simulated maximum and average T_i in D10 and D17.

Indoor air temperature (°C)	D10 (Shown also in Table 8)	D17
Maximum	36.61	31.30
Average	26.90	25.39
AVE_{day}	28.93	26.82

The indoor and outdoor air temperatures for D10 and D18 on two different selected days but of similar outdoor air temperatures and variation patterns are comparatively shown in Fig. 13. As seen, for both days, the daily average outdoor air temperatures were at around 27 °C. The air temperature inside the PTH in D10, $T_{i(D10)}$, was always lower than $T_{o(D18)}$ at nighttime, as shown in both Fig. 13 and Table 11. Since the PCM layer in D10 could be moved from indoor to outdoor, the PCM could therefore release heat to a colder outdoor air at nighttime, to charge the PCM but not release heat to indoor air at nighttime. Consequently, a movable PCM-based energy storage system, as represented by D10, was preferred for improving PTH's indoor thermal environment at daytime in summer.

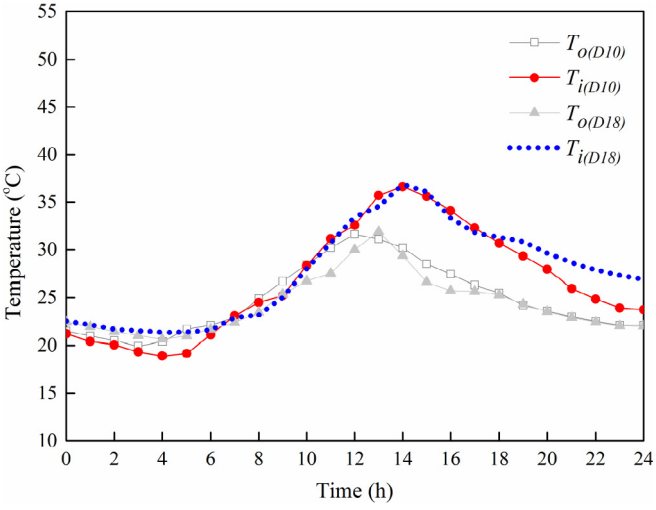

Fig. 13. Comparisons of indoor and outdoor air temperatures in D10 and D18.

Table 11
The maximum, minimum and average indoor air temperatures in D10 and D18.

Indoor air temperature (°C)	D10	D18
Maximum	36.61	36.89
Minimum	18.93	21.37
Average	26.90	27.56

4. Conclusions

This paper reports a numerical study on optimizing the designs of applying PCM to a full-scale disaster-relief PTH in order to improve its indoor thermal environment in summer. The numerical study included two parts: 1) optimizing designs of applying PCMs at different positions relative to PTH's envelopes for improved indoor thermal environment at daytime in summer and 2) an analysis on the impacts of the amount of PCM used on its indoor thermal environment.

In the first part, in order to find the best design of applying PCM to a PTH, a total of 16 designs to place PCM at different positions relative to the PTH's envelopes were defined and simulation studies with the 16 designs carried out. The study results demonstrated that in summer, D4, D7, D10, D13 and D16, among the 16 designs, can lead to better thermal environment inside the PTH, than all the other designs, because in D4, D7, D10, D13 and D16, PCM was placed on the indoor side of all envelope components and may be moved to outside the PTH for charging the PCM with cooling energy from both the sky radiation and a low temperature outdoor air at nighttime. Based the simulation results, D10, i.e., the design with PCM placed indoor at daytime and moved to outdoor at nighttime was identified as the most effective one among all the designs, and could result in the highest numbers of acceptable hour which was defined as an hour during which the air temperature inside a PTH was below the occupants' tolerant temperature in temporary shelters following a natural disaster.

In the second part, the simulation results based on D10 demonstrated that increasing PCM's thickness from 0 to 20 mm would have noticeable improvements in the thermal environment inside the PTH, but to beyond 20 mm, negligible effect on further improving indoor thermal environment. Hence, the thickness of 20 mm for PCM was recommended as a reference design value for future practical applications. The study results also suggested that it would be more effective to distribute a fixed amount of PCM to all envelope surfaces, rather than to simply place the fixed amount of PCM to just one particular envelope element.

Furthermore, the novelty of the paper includes developing and experimentally validating an EnergyPlus based mathematical model for a disaster-relief PTH, and the use of the model to find out the optimized design of applying PCM to the PTH for improving its summer daytime indoor thermal comfort. Although a related experimental study was previously reported, where a very limited number of designs of applying PCM were examined, in the current paper, by numerical simulation using the validate model, 16 different designs were examined and the best one identified for guiding future practical applications. The EnergyPlus based model was actually experimentally validated using the data collected from the experimental PTH established in the previous experimental study. In addition, the outcomes of the numerical study should be applicable not only to the case study experimental building in Chengdu, China, but also to any other buildings located in different climate zones, by using different building configurations and weather parameters in the EnergyPlus based model for the PTH. Lastly, for the optimized design, PCM layer is actually movable and may therefore be moved to outside a PTH in winter should this become necessary to avoid any negative impacts the PCM layer may have on indoor thermal environment in winter time.

Acknowledgements

The authors gratefully acknowledge the financial supports from The Hong Kong Polytechnic University, Hong Kong Jockey Club, and Sichuan University.

References

[1] Gunawardena T, Ngo T, Mendis P, Aye L, Crawford R. Time-efficient post-disaster housing reconstruction with prefabricated modular structures. Open House Int 2014;39(3):59–69.
[2] Tang A, Kwasinski A, Yu K. A longitudinal study of Tohoku telecommunication network three years after the great east Japan earthquake and tsunami. Congress on Technical Advancement 2017: Infrastructure Resilience and Energy 2017:135–42.
[3] Aye L, Ngo T, Crawford RH, Gammampila R, Mendis P. Life cycle greenhouse gas emissions and energy analysis of prefabricated reusable building modules. Energy Build 2012;47:159–68.
[4] Tas N, Tas M, Cosgun N. Permanent housing production process after 17 august 1999 marmara earthquake in Turkey. Int J Strateg Prop Manag 2011;15(3):312–28.
[5] Chang Y, Wilkinson S, Potangaroa R, Seville E. Resourcing challenges for post-disaster housing reconstruction: a comparative analysis. Build Res Inf 2010;38(3):247–64.
[6] Wang CX, Huang X, Deng SM, Long ES, Niu JL. An experimental study on applying PCMs to disaster-relief prefabricated temporary houses for improving internal thermal environment in summer. Energy Build 2018;179:301–10.
[7] Asefi M, Sirus FA. Transformable shelter: evaluation and new architectural design proposals. Procd Soc Behv 2012;51:961–6.
[8] Caia G, Ventimiglia F, Maass A. Container vs. dacha: the psychological effects of temporary housing characteristics on earthquake survivors. J Environ Psychol 2010;30(1):60–6.
[9] Dikmen N, Elias-Ozkan ST, Davidson C. Comparison of post-disaster housing procurement methods in rural areas of Turkey. Open House Int 2012;37(1):28–39.
[10] Huang LH, Long ES, Ouyang JL. Measurement of the thermal environment in temporary settlements with high building density after 2008 Wenchuan earthquake in China. In: 9th International symposium on heating, ventilation and air conditioning (Ishvac) joint with the 3rd International conference on building energy and environment (cobee), vol. 121; 2015. p. 95–100.
[11] Zhang HB, Liu J, Li CN, Lian ZW. Long-term investigation of moisture environment in underground civil air defence work. Indoor Built Environ 2017;26(6):744–57.
[12] Wang Y, Long ES, Deng SM. Applying passive cooling measures to a temporary disaster-relief prefabricated house to improve its indoor thermal environment in summer in the subtropics. Energy Build 2017;139:456–64.
[13] Wang Y, Wang L, Long ES, Deng SM. An experimental study on the indoor thermal environment in prefabricated houses in the subtropics. Energy Build 2016;127:529–39.
[14] Mazzeo D, Oliveti G. Thermal field and heat storage in a cyclic phase change process caused by several moving melting and solidification interfaces in the layer. Int J Therm Sci 2018;129:462–88.
[15] Sage-Lauck JS, Sailor DJ. Evaluation of phase change materials for improving thermal comfort in a super-insulated residential building. Energy Build 2014;79:32–40.
[16] Figueiredo A, Vicente R, Lapa J, Cardoso C, Rodrigues F, Kampf J. Indoor thermal comfort assessment using different constructive solutions incorporating PCM. Appl Energy 2017;208:1208–21.
[17] Alam M, Sanjayan J, Zou PXW, Ramakrishnan S, Wilson J. Evaluating the passive and free cooling application methods of phase change materials in residential buildings: a comparative study. Energy Build 2017;148:238–56.
[18] Song M, Niu F, Mao N, Hu Y, Deng S. Review on building energy performance improvement using phase change materials. Energy Build 2018;158:776–93.
[19] Pomianowski M, Heiselberg P, Zhang YP. Review of thermal energy storage technologies based on PCM application in buildings. Energy Build 2013;67:56–69.
[20] Soares N, Costa JJ, Gaspar AR, Santos P. Review of passive PCM latent heat thermal energy storage systems towards buildings' energy efficiency. Energy Build 2013;59:82–103.
[21] Silva T, Vicente R, Rodrigues F. Literature review on the use of phase change materials in glazing and shading solutions. Renew Sustain Energy Rev 2016;53:515–35.
[22] PCMs for Residential Building Applications. A short review focused on disadvantages and proposals for future development. Buildings 2017;7(3):78.
[23] Zhou D, Zhao CY, Tian Y. Review on thermal energy storage with phase change materials (PCMs) in building applications. Appl Energy 2012;92:593–605.
[24] Kenisarin M, Mahkamov K. Passive thermal control in residential buildings

using phase change materials. Renew Sustain Energy Rev 2016;55:371–98.
[25] Tyagi VV, Buddhi D, Kothari R, Tyagi SK. Phase change material (PCM) based thermal management system for cool energy storage application in building: an experimental study. Energy Build 2012;51:248–54.
[26] Tyagi VV, Pandey AK, Buddhi D, Tyagi SK. Exergy and energy analyses of two different types of PCM based thermal management systems for space air conditioning applications. Energy Convers Manag 2013;69:1–8.
[27] Lin W, Ma Z, Cooper P, Sohel MI, Yang L. Thermal performance investigation and optimization of buildings with integrated phase change materials and solar photovoltaic thermal collectors. Energy Build 2016;116:562–73.
[28] Weinläder H, Klinker F, Yasin M. PCM cooling ceilings in the Energy Efficiency Center—passive cooling potential of two different system designs. Energy Build 2016;119:93–100.
[29] Mazzeo D, Oliveti G, Arcuri N. Definition of a new set of parameters for the dynamic thermal characterization of PCM layers in the presence of one or more liquid-solid interfaces. Energy Build 2017;141:379–96.
[30] Mazzeo D, Oliveti G, de Gracia A, Coma J, Solé A, Cabeza LF. Experimental validation of the exact analytical solution to the steady periodic heat transfer problem in a PCM layer. Energy 2017;140:1131–47.
[31] Saffari M, de Gracia A, Fernandez C, Cabeza LF. Simulation-based optimization of PCM melting temperature to improve the energy performance in buildings. Appl Energy 2017;202:420–34.
[32] Zhang Y, Long E, Li Y, Li P. Solar radiation reflective coating material on building envelopes: heat transfer analysis and cooling energy saving. Energy Explor Exploit 2017;35(6):748–66.
[33] Costanzo V, Evola G, Marletta L. Energy savings in buildings or UHI mitigation: Comparison between green roofs and cool roofs. Energy Build 2016;114:247–55.
[34] Morakinyo TE, Dahanayake KWDKC, Ng E, Chow CL. Temperature and cooling demand reduction by green-roof types in different climates and urban densities: a co-simulation parametric study. Energy Build 2017;145:226–37.
[35] Karachaliou P, Santamouris M, Pangalou H. Experimental and numerical analysis of the energy performance of a large scale intensive green roof system installed on an office building in Athens. Energy Build 2016;114:256–64.
[36] Foustalieraki M, Assimakopoulos MN, Santamouris M, Pangalou H. Energy performance of a medium scale green roof system installed on a commercial building using numerical and experimental data recorded during the cold period of the year. Energy Build 2017;135:33–8.
[37] Silva CM, Gomes MG, Silva M. Green roofs energy performance in Mediterranean climate. Energy Build 2016;116:318–25.
[38] Zeng C, Bai XL, Sun LX, Zhang YZ, Yuan YP. Optimal parameters of green roofs in representative cities of four climate zones in China: a simulation study. Energy Build 2017;150:118–31.
[39] Inman RH, Pedro HTC, Coimbra CFM. Solar forecasting methods for renewable energy integration. Prog Energ Combust 2013;39(6):535–76.
[40] Yan W. Experimental and numerical studies on improving the indoor thermal environment in a disaster-relief temporary prefabricated house located in the subtropics, PhD Thesis. The Hong Kong Polytechnic University; 2016.
[41] ASHRAE. International weather for energy calculations, IWEC weather files atlanta. ASHRAE; 2001.
[42] ASHRAE. ASHRAE handbook fundamentals, American society of heating. Atlanta, GA: Refrigerating and Air-Conditioning Engineers Inc.; 2013.
[43] ASHRAE. ANSI/ASHRAE standard 55–2013. In: Thermal environmental conditions for human occupancy; 2013.